A Molecular Dynamics Investigation of Lipid Bilayer Perturbation by PIP_2

Dmitry Lupyan,[†] Mihaly Mezei,[†] Diomedes E. Logothetis,[†‡] and Roman Osman[†*]
[†]Department of Structural and Chemical Biology, Mount Sinai School of Medicine, New York, New York; and [‡]Department of Physiology and Biophysics, Virginia Commonwealth University, School of Medicine, Richmond, Virginia

ABSTRACT Phosphoinositides like phosphatidylinositol 4,5-*bis*phosphate (PIP_2) are negatively charged lipids that play a pivotal role in membrane trafficking, signal transduction, and protein anchoring. We have designed a force field for the PIP_2 headgroup using quantum mechanical methods and characterized its properties inside a lipid bilayer using molecular dynamics simulations. Macroscopic properties such as area/headgroup, density profiles, and lipid order parameters calculated from these simulations agree well with the experimental values. However, microscopically, the PIP_2 introduces a local perturbation of the lipid bilayer. The average PIP_2 headgroup orientation of 45° relative to the bilayer normal induces a unique, distance-dependent organization of the lipids that surround PIP_2. The headgroups of these lipids preferentially orient closer to the bilayer normal. This perturbation creates a PIP_2 lipid microdomain with the neighboring lipids. We propose that the PIP_2 lipid microdomain enables the PIP_2 to function as a membrane-bound anchoring molecule.

INTRODUCTION

Phosphatidylinositol is a lipid molecule found in the cytosolic leaflet of the cell plasma membrane and in the membranes of several intracellular organelles. Its phosphorylated derivatives are known as phosphoinositides (PIPs) (1). PIPs have two hydrocarbon tails, arachidonate and stearate, which are connected through a glycerol group to the inositol headgroup. Three phosphorylation sites on the 3, 4, and 5 positions of the inositol ring give rise to seven distinct combinations of mono-, bis-, and tris-phosphorylated products. Inside the cell, phosphoinositide turnover is tightly controlled by metabolic regulatory enzymes such as specialized kinases, phosphatases, and phospholipases. Defects in phosphoinositide metabolism are associated with disorders such as cancer, cardiovascular disease, and autoimmune dysfunction (2,3).

Depending on the cell type, PIPs constitute ~1–2% of the total phospholipids in the plasma membrane. Despite their low membrane content, PIPs are known to spatially sequester into PIP-enriched rafts, and thus, the local concentration of PIPs varies dramatically (4,5). Inside the cell, the products of phosphoinositide metabolism are key membrane signaling molecules that play an important role in numerous intracellular signaling pathways. For example, the most abundant PIP is $PI(4,5)P_2$ (commonly abbreviated as PIP_2 (Fig. 1 *A*)), which has long been considered to act as a ubiquitous second messenger and as a precursor to other second messengers, such as diacylglycerol (DAG), D-myo-inositol 1,4,5-trisphosphate (IP_3), and phosphatidylinositol 3,4,5-trisphosphate (PIP_3) (3,6,7). More recently, it was also suggested that PIP_2 may have some intrinsic catalytic activity (8). Another widely recognized functional role of PIP_2 and other PIPs is as substrates for a variety of PIP-effector proteins. All PIP-adhesion proteins have a specialized domain through which they bind PIPs with various degrees of selectivity. Though a number of structures of different PIP-interacting domains have been solved (free and in complex), the basis of protein-PIP stereoselectivity remains elusive (9).

At this time, a combination of biochemical, diffraction, and spectroscopic techniques are widely used to study PIP_2 synthesis, aggregation/sequestration, cell localization, and interactions with proteins. These techniques provide a wealth of information about the macroscopic properties of PIP_2 (10). Computational techniques, on the other hand, can be used to explore the microscopic behavior of PIPs. In this work, we present atomic-resolution results from molecular dynamics (MD) simulations of PIP_2 in a lipid bilayer. Because the data extracted from such studies closely agrees with the available experimental data, MD simulation is a good tool for studying various aspects of lipid behavior that are not easily measurable through experimental work (11–15).

Several studies have used MD simulations to explore the interactions of PIP_2 with specific residues of peptides and proteins (16–20), and one study explores the dynamic differences between PIP_2 and phosphatidylinositol 3,4,5-trisphosphate inside the bilayer (21). Another study suggests that the lipids that surround PIP_2 also play a significant role in protein interactions; it is thought that these lipids facilitate penetration of PIP_2-interacting proteins into the bilayer by forming additional hydrogen bonds with the protein (18). In this work, we investigate the interaction of PIP_2 with neighboring lipids and its organization within the lipid bilayer. We first design force field parameters for the phosphoinositide headgroup to enable further investigation with MD simulation. To understand how PIP_2 carries out such a wide variety of biological functions, we simulate PIP_2 inside the lipid bilayer and characterize its molecular, structural, and dynamic properties. We also show and

Submitted June 15, 2009, and accepted for publication September 29, 2009.

*Correspondence: roman.osman@mssm.edu

Editor: Reinhard Lipowsky.

0006-3495/10/01/0240/8 $2.00

doi: 10.1016/j.bpj.2009.09.063

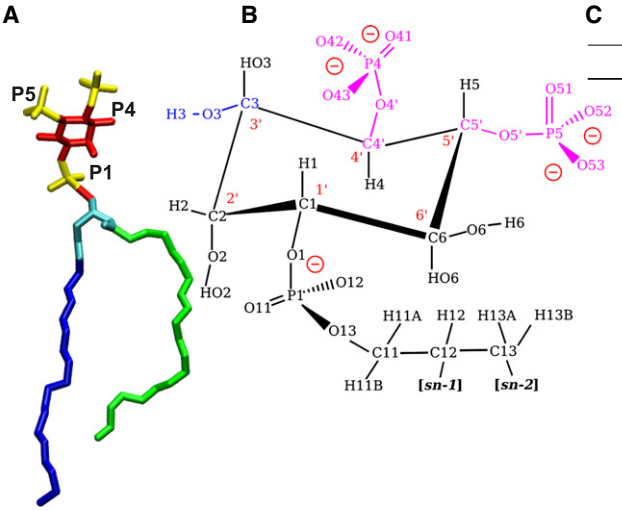

Atom(s) Name	Partial Charge
C1 - C6	0.06
O1	-0.55
O2 - O6	-0.57
H1 - H6	0.12
HO2 - HO6	0.40
P1	1.20
P3,P4,P5	1.44
O31,O32,O33	-1.03
O41,O42,O43	-1.03
O51,O52,O53	-1.03
O11,O12	-0.86
O13	-0.51
C3',C4',C5'	0.08
O3',O4',O5'	-0.54

FIGURE 1 (*A*) Heavy atom representation of a PIP_2 lipid molecule. The inositol headgroup is red; phosphates are yellow, the glycerol connecting the headgroup to the acyl chains is cyan, and the arachidonate and stearate acyl chains are green and blue, respectively. (*B*) Schematic of the PIP_2 headgroup with the nomenclature of the atom names. To change the phosphorylation state of the phosphoinositides, the force fields have been designed such that a hydroxyl group (*blue*) can be replaced by a phosphate group (*magenta*). (*C*) Partial charges correspond to atom names in *B*.

describe how PIP_2 induces the formation of a PIP_2 lipid microdomain by reorganizing the neighboring lipids in a unique way. We speculate that the formation of such microdomains is an important property of PIP_2, allowing it to act as a membrane-anchoring molecule.

COMPUTATIONAL METHODS

Lipid system setup

The coordinates of the preequilibrated 1,2-dipalmitoyl-*sn*-glycero-3-phosphocholine (DPPC) membrane patch at 323.15 K were obtained from the website of Dr. Jeffrey B. Klauda, with an initial box size of 48.0 × 48.0 × 66.118 Å (22). The membrane system contained 72 DPPC lipid molecules (36 in each leaflet), to which 150 mM of KCl and ~3400 TIP-3 water molecules were added. To prepare the simulations containing a phosphoinositide, a single DPPC molecule in the pure DPPC membrane patch was replaced by a phosphatidylinositol molecule, and two phosphate groups were added to positions 4 and 5 on the inositol headgroup. Furthermore, additional counterions were added to neutralize the system. The average size of all the systems was ~20,000 atoms.

Molecular dynamics simulations

Each lipid-water molecular system was minimized for 2000 minimization steps using the conjugate gradient method. The system was then heated for 200 ps, during which the temperature slowly increased from 0 to 330 K by rescaling the velocities every 1000 steps until the target temperature was reached. All MD simulations and minimizations were run with NAMD2.6 (23) using the CHARMM27 (24) force field that included our parameters for PIP_2. Orthorhombic periodic boundary conditions (PBC) were used to reduce boundary surface effects. The particle mesh Ewald (PME) method was used to represent long-range electrostatics with maximum grid-point spacing set to 1 Å (25). The cutoff radius for Lennard Jones interactions was 12 Å, with a smooth switching function starting at 10 Å and a nonbonded "pairlist" distance of 14 Å. The RATTLE algorithm was used to constrain all bonds involving hydrogen atoms, allowing the 2-fs time steps (26). Since the initial membrane coordinates were adopted from the preequilibrated lipid bilayer patch, each system underwent only a 10-ns equilibration run and a 50-ns production run under semi-isothermal-isobaric ($NP(x = y)T$) conditions (see Fig. S2 in the Supporting Material for the system's equilibration profile). The temperature was kept constant at 330 K by using Langevin dynamics, and a Nosé-Hoover Langevin piston was used for pressure control at 1 bar (27,28). The simulations were run at temperatures above the DPPC gel-liquid transition phase (29,30).

2D radial distribution function

The two-dimensional radial distribution function ($g_{2D}(r)$) available in GROMACS was used to characterize the lateral radial distribution of lipids in the bilayer plane (31). In this method, the counting and distances are calculated in the *x-y* plane, disregarding the *z* axis.

Lipid pulling

To show that adhesion forces that resist the extraction of a lipid molecule from a bilayer are greater for PIP_2 than for a typical lipidlike DPPC, we performed an atomic force microscopy (AFM)-type pulling through MD simulations. Steered molecular dynamics (SMD) has been employed to simulate the extraction of a PIP_2 and DPPC lipid molecules from DPPC bilayers. Previous works have shown that SMD results agree well with the experimental AFM data (32–34). In SMD simulations, a macromolecular system is subjected to user-defined external forces chosen to induce a reaction on a nanosecond timescale. In our simulations, the external force we applied was to the phosphorus atom of a lipid. The phosphorus atom (P in DPPC, or P1 in PIP_2) was harmonically restrained with a force constant k to a point moving away along the normal to the surface of the lipid bilayer with a constant velocity (v), which caused the lipid to be pulled out from the membrane into the aqueous environment. The absolute value of the external force acting on the lipid is given by $F(x,t) = k(vt - x)$, where x is the displacement of the restrained atom, $v = 0.0005$ Å/ps, and $k = 0.25$ kcal/mol·Å^2.

Analysis, visualization, and graphing tools

Quantum mechanical (QM) visualization and analysis was performed using Molden. Molecular visualization and system setup was done with VMD and its library of plug-ins. PIP_2 conformation modeling was performed with Maestro (Schrödinger, Portland, OR). Simulation post-processing and analysis was performed with VMD scripting, GROMACS, and Simulaid (31,35–37). Plots were generated using XMGrace (http://plasma-gate.weizmann.ac.il/Grace).

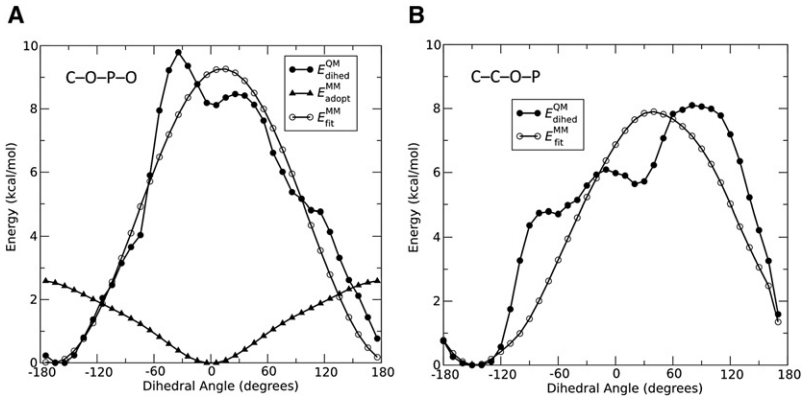

FIGURE 2 A parameterization of the torsional potentials for dihedral angles C-O-P-O (*A*) and C-C-O-P (*B*). E^{QM}_{dihed} is a QM torsional potential calculated with PES; E^{MM}_{fit} is the fitted molecular mechanical potential energy; and E^{MM}_{adopt} is the torsional potential for dihedral angle in *A* adopted from the Charmm27 parameter set.

RESULTS

Parameterization of phosphatidylinositol headgroup

The atomic charges and the geometrical conformation of the phosphatidylinositol headgroup were obtained using QM methods. Geometry optimization and distribution of partial charges on the surface of the phosphatidyl-inositol headgroup (IP) were calculated using Gaussian03 (38) at Hartree-Fock level of theory with a 6-31G+* basis set. The partial atomic charge distribution of IP was derived using the RESP package (39), which fits the charges to reproduce the electrostatic potential on the surface of the molecule obtained from the wavefunction (Fig. 1, *B* and *C*). Electronic properties were calculated with the polarized continuum model, representing water as an implicit solvent with a dielectric constant of 80 using Pauling's atomic radii and 1.2 as the scaling factor for the definition of the solvent-accessible surfaces (40–42). The parameterization strategy for IP, described here, is consistent with the methodology employed in the CHARMM27 lipid force field.

Some studies reveal that under physiological conditions, PIP_2 is protonated on one of the two phosphates (43,44), whereas other studies suggest that the net charge of PIP_2 is $-3e$, due to a presumed binding of either H^+ or K^+ ions to the phosphates (45,46). Since all of our MD simulations contain explicit ions (KCl), we parameterized PIP_2 in an unprotonated state with a net charge of $-5e$.

Since there are seven distinct forms of phosphoinositides—PI(3)P, $PI(3,4)P_2$, $PI(3,4,5)P_3$, $PI(3,5)P_2$, PI(4)P, PIP_2, PI(5)P—whose net charge ranges from $-3e$ to $-7e$, we designed our force field such that the phosphate charges are transferable, thus avoiding the need to reparametrize each PIP. The net charge of the phosphoinositide is adjusted in increments of $-2e$, which corresponds to the substitution of a hydroxyl group (R-OH) by a phosphate group (R-O-PO_3^{2-}). Force-field parameters for the glycerol, arachidonate, and stearate groups were adopted from the standard CHARMM27 parameter set (24,47,48).

The interactions of the phosphatidylinositol headgroup with the glycerol part of the lipid are largely governed by the dihedral potential connecting these two chemical groups. The torsional parameters adopted from the CHARMM27 force field set did not correctly describe the potential between these two chemical groups. This can be seen in Fig. 2 *A*, where the the torsional parameters (E^{MM}_{fit}) from the CHARMM27 parameter set suggest incorrect minima value. To characterize these interactions, we reparameterized two key torsional angles—C-O-P-O and C-C-O-P (C1-O1-P1-O13 and {C2;C6}-C1-O1-P1 in Fig. 1 *B*)—using a highly accurate torsional energy scan from the QM calculations. The optimized structure of the PI headgroup was subjected to a potential energy surface (PES) scan along the internal coordinates of these torsional angles. All atoms except those involved in the torsion angle studied were kept fixed during the scan. The determination of the conformational minimum was scanned in 10° intervals with respect to each torsional motion (see Fig. 2, *A* and *B*). The Hartree-Fock level of theory with 6-31G+* basis set was used in PES.

The QM torsional potential energy (E^{QM}_{dihed}) was fitted to the molecular mechanical torsional potential energy (E^{MM}_{fit}), expressed as

$$E^{MM}_{dihed} = \sum k_n(1 + \cos(n \times \theta - \gamma_n)). \quad (1)$$

The QM torsional potential energy along θ was calculated using

$$E^{QM}_{dihed}(\theta) = E^{QM}(\theta) - E^{MM}_{null}(\theta), \quad (2)$$

where E^{MM}_{null} is the functional form of the CHARMM27 force field, with $k_n = 0$ for the dihedral potential. In Fig. 2, we show the E^{QM}_{dihed}-fitted C-O-P-O and C-C-O-P torsional potentials (E^{MM}_{fit}) with the single Fourier series terms $k = 4.64$ kcal/mol; $\gamma = 12.30$ and $k = 4.30$ kcal/mol; $\gamma = -20.00$, respectively.

Simulations of PIP_2 in a lipid bilayer

To characterize the properties of PIP_2 in the lipid bilayer, we ran a 50-ns MD simulation of a single PIP_2 molecule in a patch of DPPC membrane. As a control, we also simulated

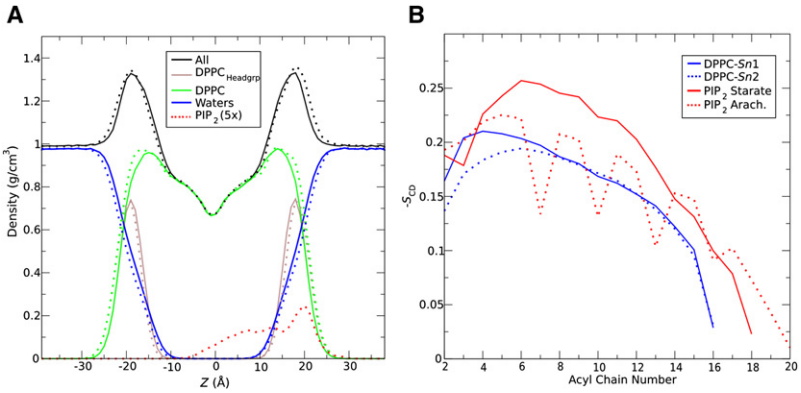

FIGURE 3 (*A*) Density profiles for the DPPC system (*solid lines*) and PIP_2-containing system (*dashed lines*) along the axis orthogonal to the bilayer (z axis). The overall density profile of the system is shown in black. The component densities are color-coded as follows: *blue*, water; *green*, lipids; *gray*, lipid headgroups (DPPC); and *red*, PIP_2 (magnified fivefold for clarity). (*B*) The lipid order parameters ($-S_{CD}$) of DPPC and PIP_2 lipids, shown in blue and red, respectively.

a membrane patch of DPPC lipid bilayer (see Methods for simulation details). To validate the quality of our simulations, and to characterize perturbations and the effect of the PIP_2 on the lipid bilayer properties, we describe in detail key macroscopic properties of the lipid systems.

Density profiles

The density profiles of the system were calculated along the normal to the bilayer plane (Fig. 3 *A*). The total density is partitioned into water, lipids, and lipid headgroups. As expected, the density of water in the center ($Z = 0$) of a lipid hydrophobic core is zero. The symmetric density of lipids suggests that individual lipid molecules form a bilayer with low density in the hydrophobic region and high density around the headgroups. The headgroup densities can also be used to estimate the thickness of the bilayer as 37–38 Å, a value consistent with the experimentally measured value for a DPPC membrane (15). The asymmetric density of PIP_2 indicates that it resides only on one leaflet ($Z > 0$) of the lipid bilayer. Comparing the density profiles of the two systems, we observe a slight perturbation by the replacement of a single DPPC with PIP_2 lipid. This change accounts for only 2% of the difference in the system density.

Area/lipid

The area of lipid systems can be measured by ^{2}H-NMR spectroscopy (49,50). These measurements can be directly compared with the area/lipid calculated from simulations of a lipid bilayer (Table 1). The macroscopic area/lipid is lightly larger in the simulations without PIP_2 (65.24 ± 0.11 Å^2) than in the PIP_2-containing simulation (64.87 ± 0.08 Å^2), and both of these values are consistent with previous simulations of DPPC membranes (15,51). This small contraction of ~0.5% is statistically significant, and it may represent a real PIP_2-induced effect. However, the range of the experimental area/lipid headgroup for DPPC bilayers varies from 56 to 72 Å^2 (15,29,50–52). The main difficulty in measuring this property experimentally is that the the measurements are sensitive to multiple physicochemical conditions, such as temperature, ionic concentration, hydration level, and external lateral tension on the bilayer. All this suggests that it may be technically difficult to experimentally discern an effect of PIP_2 on the total area of the membrane patch.

Lipid order parameter

The lipid order parameters ($-S_{CD}$) quantify the relative order of the hydrocarbon tails. This is calculated from the MD trajectory using Eq. 3 and can be directly compared with the experimentally determined values obtained through quadrupole splitting measurements (15).

$$S_{CD}^{(i)} = \frac{1}{2}\langle 3\cos^2\theta_i - 1\rangle. \quad (3)$$

S_{CD} is calculated for each acyl group i, where θ_i is the angle between the C_i-H_i molecular axis and the normal of the bilayer. The order parameters of the DPPC's *sn*-1 and *sn*-2 acyl chains have been calculated for each system (Fig. 3 *B*). Both chains show a ''plateau'' at ~0.20 in carbons 2–6, a feature highly consistent with experimental measurements (49,52). In Fig. 3 *B*, we also show the calculated $-S_{CD}$ of the PIP_2 naturally occurring acyl chains arachidonate and stearate. Note that the acyl chains closer to the glycerol group are chemically identical, but that the stearate in PIP_2 exhibits

TABLE 1 Calculated properties of bilayer systems

Property	DPPC	DPPC + PI(4,5)P_2
Charge	0	−5
Area/lipid (Å^2)*	65.24 ± 0.11	64.87 ± 0.09
Bilayer thickness (Å)†	37.40 ± 0.30	37.65 ± 0.27
Headgroup protrusion (Å)‡	1.16 ± 1.70	5.99 ± 1.26; 5.10 ± 1.21
Headgroup orientation (°)§	77.29 ± 21.53	41.84 ± 10.51

*Area/lipid is calculated by dividing the xy area of the lipid patch by the number of lipid molecules (36).
†Bilayer thickness is measured from the average distance of DPPC phosphorus atoms in the adjacent leaflets.
‡For PIP_2, headgroup protrusion measures the angle between the 2-hydroxyl group and the normal to the bilayer plane; for DPPC, it measures the pseudoangle between the P-N bond and the normal to the bilayer plane.
§Headgroup protrusion is the Z-component of the distance between P-N atoms (for DPPC) and the average of P1-P4; P1-P5 atoms (for PIP_2).

a higher degree of order in the ''plateau'' region than the *sn*-1 in DPPC. Differences between these two chemically identical regions must be affected by the packing of lipids. An enhanced ordering of the acyl chains is associated with a reduction in the area/lipid (53).

Lipid organization

To analyze the effect of PIP_2 on lipid organization, we calculated the $g_{2D}(r)$ of lipids around DPPC and PIP_2 molecules in the *x*-*y* plane. In Fig. 4 *A*, we investigate the pair distribution of central phosphorus atoms in a single leaflet. In agreement with other studies, we observe that around any single DPPC molecule, the other DPPC lipids are organized with a degree of periodicity—two lipid shells whose minima occur at $r \approx 7.6$ Å and 10.1 Å, respectively (51,53). In contrast, the distribution of DPPC lipids around a PIP_2 shows only one pronounced shell at $r \approx 7.8$ Å and whose peak is at $r \approx 6.1$ Å (0.51 Å closer than in the case of DPPC lipids). The second lipid shell maximum shifted to $r \approx 11.4$ Å due to the fact that the semi-head-tail organization of the DPPC molecules within the membrane plane had been perturbed by PIP_2 and the high local concentration of ions. Overall, these results suggest that PIP_2 induces a rearrangement that increases the organization of the DPPC lipids that surround it.

We further investigated the rearrangement of the lipids surrounding the PIP_2 by calculating the tilt of a PC headgroup with respect to the normal of the bilayer. The results of this analysis are shown in Fig. 4 *B*. The average P-N pseudoangle in the DPPC system is $77.29 \pm 21.53°$, which indicates that the DPPC headgroups lie nearly parallel to the bilayer. In contrast, in the PIP_2-containing patch, the DPPC lipids that are in direct contact with PIP_2 adopt a headgroup conformation nearly normal to the bilayer. This DPPC headgroup conformation is not observed in the pure DPPC membrane, which suggests that it is induced by PIP_2 (see schematic in Fig. 4 *C*). The DPPC headgroups within 7.5–9.5 Å of the PIP_2 molecule adopt similar conformations to the headgroups in the pure DPPC membrane, except that they exhibit a wider angle tilt distribution, $74.13 \pm 29.60°$. This distribution difference is attributed to the absence of the organization of the lipids around PIP_2 in the range 7.5–9.5 Å, as can be observed in pure DPPC membranes (see Fig. 4, *A* and *C*). Since PIP_2 often acts as a membrane-bound anchoring lipid for proteins (9), we hypothesize that the described rearrangement and organization of the lipids that surround the PIP_2 generate the environment that provides the PIP_2 with better packing within the membrane and a resistance to vertical displacement by anchoring proteins.

PIP_2 headgroup orientation

The orientation and position of the PIP_2 headgroup largely depend on its interaction with the solvent. Understanding these interactions and their effect on the headgroup conformation may lead us to understand how the PIP_2 charged groups are presented to the proteins they interact with. In previous studies, headgroup orientation was modeled by fitting the data obtained from combinations of the nuclear Overhauser effect (NOE) and dipolar coupling NMR spectroscopy experiments (54–58). These models predict a completely erect PIP_2 headgroup, where the plane of the inositol ring is orthogonal to the membrane plane. This conformation was believed to be ''locked in'' by the intramolecular hydrogen bonds between either the 2- or the 6-hydroxyl group, or both, and the oxygens on the P1 phosphate group. We monitored the hydrogen-bond formation between these two groups throughout our simulation. We found that only the 6-hydroxyl group interacts with the phosphate. This hydrogen bond between the 6-hydroxyl and either the pro-R or pro-S oxygens of the phosphate was present ~87% of the simulation time (Fig. S2 *A*).

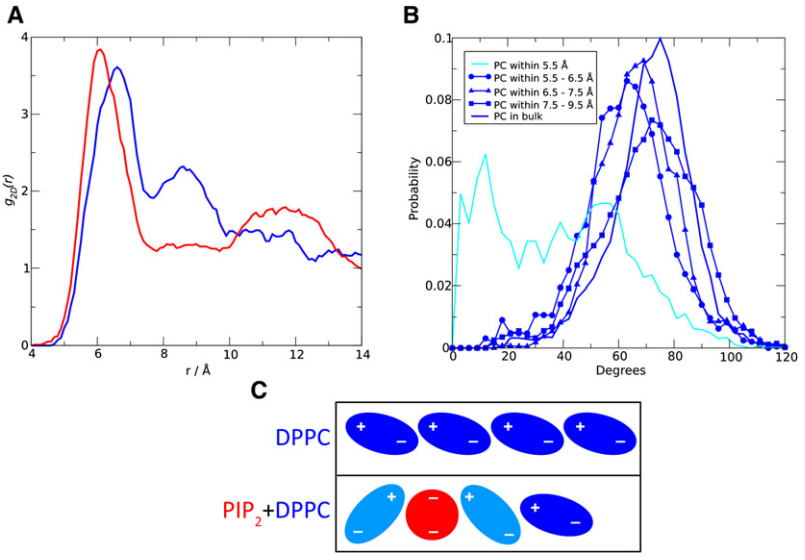

FIGURE 4 (*A*) Planar $g_{2D}(r)$ of the phosphorus atoms in the DPPC bilayer (*blue*) and within 14 Å of PIP_2 (*red*). Please see Computational methods for calculation description. (*B*) Distribution of the DPPC headgroup tilt grouped according to distance from the PIP_2 lipid. (*C*) A schematic of the DPPC headgroups in a pure DPPC membrane and in a membrane with PIP_2 lipid.

Our simulation reveals that the 2-hydroxyl forms a hydrogen bond with a phosphate group of the neighboring lipid ~61% of the simulation time (Fig. S2, *B* and *C*).

The PIP_2 headgroup orientation was previously described as a series of four torsional angles between the atoms of the glycerol, the phosphate, and the inositol ring (C12-C11-O13-P1-O1-C1-C6 atoms in Fig. 1 *B*). From neutron diffraction scattering data, these torsional angles were believed to adopt a *trans*, *trans*, *trans*, *gauche*$^-$ conformation, whereas in our simulations, we monitored these angles and observed that they are in the *trans*, *trans*, *gauche*$^+$, *trans* conformation (see Fig. S1, *A–C* (54). The conformational change in these torsional angles over the course of the simulation is illustrated in Fig. S1 *D*. In this work, we further characterize the conformation of the PIP_2 headgroup as a combination of the orientation of a key 2-hydroxyl group and the extension of the phosphates. Note that on the inositol ring, the axial 2-hydroxyl group is what makes all seven phosphoinositides stereochemically unique—all other hydroxyl groups are equatorial. The headgroup orientation is expressed as the angle between the normal of the lipid plane and the 2-hydroxyl group, ($\Theta_{Z\text{-}C2\text{-}O2}$). We calculated $\Theta_{Z\text{-}C2\text{-}O2}$ to be 41.84 $\pm$ 10.51°. The headgroup extension can further be described by the protrusion of the P4 and P5 atoms. We define the protrusion of phosphates as the *Z*-component of the distance between phosphate P4 and P5 atoms and the central P1 atom. The protrusions of the P4 and P5 atoms are 5.99 $\pm$ 1.26 Å and 5.10 $\pm$ 1.21 Å, respectively. These values are similar with those reported by Li et al. (21). If we apply the Li et al. definition to measure the DPPC headgroup protrusion (the *Z*-component of the P-N distance), we get 1.16 $\pm$ 1.70 Å.

To describe the orientation and the extension of the PIP_2 headgroup with respect to the lipid bilayer, we define three values: $\Theta_{Z\text{-}C2\text{-}O2}$ and the protrusion of the P4 and P5 atoms. In comparison with DPPC headgroups, the PIP_2 headgroup is larger and adopts a more erect conformation with respect to the normal of the bilayer. All this suggests that in addition to the change in the nature of the charge (positive and negative), the PIP_2 extends 4–6 Å farther into an aqueous phase compared to a typical phospholipid.

PIP_2 role as a membrane-bound anchor

A number of cytosolic proteins use PIP_2 lipids as anchoring molecules for localization on the membrane (9). For PIP_2 to play a role as a membrane-bound anchoring molecule, it must be more stable within the membrane bilayer than other typical lipids. We believe that the described ability of PIP_2 to form a microdomain with its neighboring lipids contributes to its stability within the bilayer. To address how tightly PIP_2 is bound in the membrane, we performed an AFM-type simulation where the lipid is vertically displaced out of the membrane environment while the force acting on it is being monitored (32,33). Using SMD, we compared the work required to pull each lipid type out of the membrane. We observed that to pull a DPPC lipid that is in direct contact with PIP_2 requires ~50% more work than to pull a DPPC lipid out of a pure DPPC bilayer (see Fig. 5). This suggests that PIP_2 forms a tight complex with the lipids with which it is in contact. We also compared the work required to pull a PIP_2 lipid out of a bilayer with that required for pulling a DPPC lipid. We observe that three times more work is required for PIP_2 pulling than for DPPC pulling, which suggests that PIP_2 would serve as a better anchoring lipid than DPPC. In fact, the interactions of the PIP_2 with its neighboring lipids are so strong that when PIP_2 is being pulled out, it pulls the surrounding DPPC lipids along with it part of the way. In Fig. 5, we can observe the breakage of two DPPC lipids away from the PIP_2 at $d \approx 12$ and 20 Å, respectively. Together with the previous results, SMD pulling experiments further suggest that the role of PIP_2 as a membrane-bound anchoring molecule is due to its increased vertical stability inside the bilayer. This vertical stability is facilitated by the lipid molecules that surround PIP_2, with which it forms lipid microdomains.

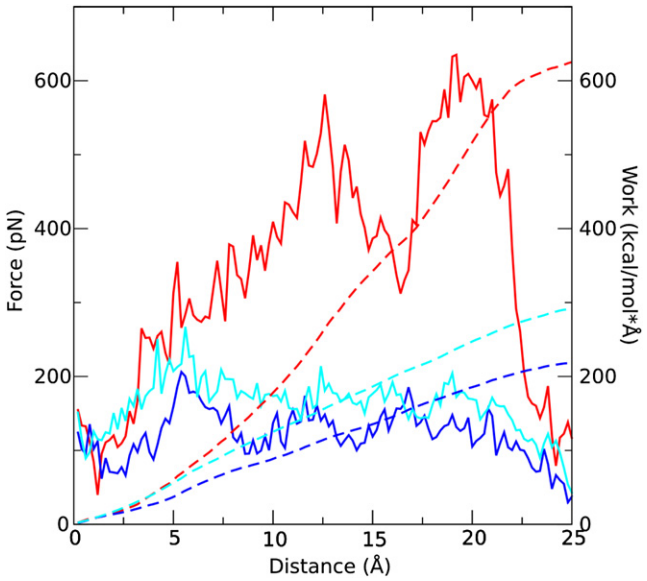

FIGURE 5 AFM-type lipid expulsion from the bilayer into the water environment. Solid lines show force and dashed lines show work required, for PIP_2 (*red*), DPPC (*blue*), and DPPC lipids near the PIP_2 (*cyan*).

DISCUSSION

In this work, we used the quantum mechanical level of theory to design the phosphoinositide parameter set compatible with the CHARMM27 force fields. We derived the dihedral potential energy for key torsional angles, as well as the partial charges for the inositol ring. Transferable partial charges of the phosphate groups were designed such that any phosphorylation state of a PI could be generated. Previous all-atom parameterizations of PIP_2 did not account

for transferability of the phosphate groups, nor were the key torsional potentials optimized (16,19). Also, the net charge of the partial charges reported in these works was unclear, as was the rationale for their design.

Generating the 4,5 configuration of the phosphates on the inositol headgroup gave rise to a PIP_2 lipid molecule. PIP_2 was embedded and simulated inside a DPPC lipid bilayer, and its dynamic behavior throughout the course of the 50-ns simulation was characterized. We systematically compared simulations of the PIP_2-containing bilayer with pure DPPC bilayer and reported that the macroscopic properties of these two systems did not significantly change, and that the area/lipid and the density profile of the two systems remained similar. However, the microscopic properties of the two systems did show significant variation in that 1), the analysis of the lipid order parameters ($-S_{CD}$) suggests that PIP_2 acyl carbons are more ordered than the equivalent carbons in the DPPC acyl chains; 2), the planar organization of DPPC is altered upon introduction of PIP_2; and 3), the DPPC headgroups in contact with PIP_2 adopted conformations that were not observed in the pure DPPC lipid simulation. These results, together with the SMD pulling experiments, suggest that PIP_2 induces a rearrangement and reorganization of the lipids around it. Together with the neighboring lipids, PIP_2 forms a stable microdomain, which lasts throughout the simulation time. We believe that the formation of the microdomains is an important property of PIP_2, which increases the force required to induce a vertical displacement and thus allows it to act as a membrane-bound anchoring molecule.

SUPPORTING MATERIAL

Two figures are available at http://www.biophysj.org/biophysj/supplemental/S0006-3495(09)01614-2.

We thank Tom Joseph for carefully reading the manuscript and for his feedback.

This work was supported in part by the Mount Sinai School of Medicine graduate program, and by the National Institutes of Health (NIH grant HL059949 to D.E.L.), and an NIH Integrative Graduate Education and Research Traineeship in Computational Biology. Computational resources were provided by the National Science Foundation TeraGrid and the Computational Biology Shared Facility of the Mount Sinai School of Medicine.

REFERENCES

1. Lemmon, M. A., and K. M. Ferguson. 2000. Signal-dependent membrane targeting by pleckstrin homology (PH) domains. *Biochem. J.* 350:1–18.
2. Pendaries, C., H. Tronchère, …, B. Payrastre. 2003. Phosphoinositide signaling disorders in human diseases. *FEBS Lett.* 546:25–31.
3. Rusten, T. E., and H. Stenmark. 2006. Analyzing phosphoinositides and their interacting proteins. *Nat. Methods.* 3:251–258.
4. McLaughlin, S., and D. Murray. 2005. Plasma membrane phosphoinositide organization by protein electrostatics. *Nature.* 438:605–611.
5. Hermelink, A., and G. Brezesinski. 2008. Do unsaturated phosphoinositides mix with ordered phosphadidylcholine model membranes? *J. Lipid Res.* 49:1918–1925.
6. Kapeller, R., and L. C. Cantley. 1994. Phosphatidylinositol 3-kinase. *Bioessays.* 16:565–576.
7. Czech, M. P. 2000. PIP2 and PIP3: complex roles at the cell surface. *Cell.* 100:603–606.
8. Bhandari, R., A. Saiardi, …, S. H. Snyder. 2007. Protein pyrophosphorylation by inositol pyrophosphates is a posttranslational event. *Proc. Natl. Acad. Sci. USA.* 104:15305–15310.
9. Rosenhouse-Dantsker, A., and D. E. Logothetis. 2007. Molecular characteristics of phosphoinositide binding. *Pflugers Arch.* 455:45–53.
10. Levental, I., A. Cebers, and P. A. Janmey. 2008. Combined electrostatics and hydrogen bonding determine intermolecular interactions between polyphosphoinositides. *J. Am. Chem. Soc.* 130:9025–9030.
11. Petrache, H. I., S. E. Feller, and J. F. Nagle. 1997. Determination of component volumes of lipid bilayers from simulations. *Biophys. J.* 72:2237–2242.
12. Pastor, R. W., R. M. Venable, and M. Karplus. 1991. Model for the structure of the lipid bilayer. *Proc. Natl. Acad. Sci. USA.* 88: 892–896.
13. Rodríguez, Y., M. Mezei, and R. Osman. 2007. Association free energy of dipalmitoylphosphatidylserines in a mixed dipalmitoylphosphatidylcholine membrane. *Biophys. J.* 92:3071–3080.
14. Feller, S. E., D. Yin, …, A. D. MacKerell, Jr. 1997. Molecular dynamics simulation of unsaturated lipid bilayers at low hydration: parameterization and comparison with diffraction studies. *Biophys. J.* 73:2269–2279.
15. Leekumjorn, S., and A. K. Sum. 2006. Molecular simulation study of structural and dynamic properties of mixed DPPC/DPPE bilayers. *Biophys. J.* 90:3951–3965.
16. Liepiņa, I., C. Czaplewski, …, A. Liwo. 2003. Molecular dynamics study of a gelsolin-derived peptide binding to a lipid bilayer containing phosphatidylinositol 4,5-bisphosphate. *Biopolymers.* 71:49–70.
17. Haider, S., A. I. Tarasov, …, F. M. Ashcroft. 2007. Identification of the PIP2-binding site on Kir6.2 by molecular modelling and functional analysis. *EMBO J.* 26:3749–3759.
18. Psachoulia, E., and M. S. Sansom. 2008. Interactions of the pleckstrin homology domain with phosphatidylinositol phosphate and membranes: characterization via molecular dynamics simulations. *Biochemistry.* 47:4211–4220.
19. Brauchi, S., G. Orta, …, R. Latorre. 2007. Dissection of the components for PIP2 activation and thermosensation in TRP channels. *Proc. Natl. Acad. Sci. USA.* 104:10246–10251.
20. Blood, P. D., R. D. Swenson, and G. A. Voth. 2008. Factors influencing local membrane curvature induction by N-BAR domains as revealed by molecular dynamics simulations. *Biophys. J.* 95:1866–1876.
21. Li, Z., R. M. Venable, …, R. W. Pastor. 2009. Molecular dynamics simulations of PIP2 and PIP3 in lipid bilayers: determination of ring orientation, and the effects of surface roughness on a Poisson-Boltzmann description. *Biophys. J.* 97:155–163.
22. Klauda, J. 2009. Molecular coordinates of preequilibrated lipid systems. http://terpconnect.umd.edu/~jbklauda/research/download.html
23. Phillips, J. C., R. Braun, …, K. Schulten. 2005. Scalable molecular dynamics with NAMD. *J. Comput. Chem.* 26:1781–1802.
24. Foloppe, N., and A. Mackerell, Jr. 2000. All-atom empirical force field for nucleic acids: I. Parameter optimization based on small molecule and condensed phase macromolecular target data. *J. Comput. Chem.* 21:86–104.
25. Darden, T., D. York, and L. Pedersen. 1993. Particle mesh Ewald: An N*log(N) method for Ewald sums in large systems. *J. Chem. Phys.* 98:10089–10092.
26. Ryckaert, J., G. Ciccotti, and H. Berendsen. 1977. Numerical integration of the cartesian equations of motion of a system with constraints: molecular dynamics of n-alkanes. *J. Comput. Phys.* 23: 327–341.

27. Feller, S., Y. Zhang, …, B. Brooks. 1995. Constant pressure molecular dynamics simulation: the Langevin piston method. *J. Chem. Phys.* 103:4613–4621.

28. Martyna, G., D. Tobias, and M. Klein. 1994. Constant pressure molecular dynamics algorithms. *J. Chem. Phys.* 101:4177–4189.

29. Nagle, J. F., and S. Tristram-Nagle. 2000. Structure of lipid bilayers. *Biochim. Biophys. Acta.* 1469:159–195.

30. Nagle, J. F., and S. Tristram-Nagle. 2000. Lipid bilayer structure. *Curr. Opin. Struct. Biol.* 10:474–480.

31. Van Der Spoel, D., E. Lindahl, …, H. J. Berendsen. 2005. GROMACS: fast, flexible, and free. *J. Comput. Chem.* 26:1701–1718.

32. Marrink, S. J., O. Berger, …, F. Jähnig. 1998. Adhesion forces of lipids in a phospholipid membrane studied by molecular dynamics simulations. *Biophys. J.* 74:931–943.

33. Stepaniants, S., S. Izrailev, and K. Schulten. 1997. Extraction of lipids from phospholipid membranes by steered molecular dynamics. *J. Mol. Model.* 3:473–475.

34. Izrailev, S., S. Stepaniants, …, K. Schulten. 1997. Molecular dynamics study of unbinding of the avidin-biotin complex. *Biophys. J.* 72:1568–1581.

35. Schaftenaar, G., and J. H. Noordik. 2000. Molden: a pre- and post-processing program for molecular and electronic structures. *J. Comput. Aided Mol. Des.* 14:123–134.

36. Humphrey, W., A. Dalke, and K. Schulten. 1996. VMD: visual molecular dynamics. *J. Mol. Graph.* 14:33–38, 27–28.

37. Mezei, M. 2009. Simulaid: simulation setup utilities. http://atlas.physbio.mssm.edu/~mezei/simulaid/.

38. Frisch, M., G. Trucks, et al.., J. Pople. 2003. Gaussian 03, revision C.02. http://www.gaussian.com.

39. Bayly, C., P. Cieplak, …, P. Kollman. 1993. RESP Package. *J. Phys. Chem.* 97:10269–10280.

40. Takano, Y., and K. Houk. 2005. Benchmarking the conductor-like polarizable continuum model (CPCM) for aqueous solvation free energies of neutral and ionic organic molecules. *J. Chem. Theory Comput.* 1:70–77.

41. Barone, V., M. Cossi, …, J. Tomasi. 1999. Effective generation of molecular cavities in polarizable continuum model by DefPol procedure. *J. Comput. Chem.* 20:1693–1701.

42. Pauling, L. 1960. The Nature of the Chemical Bond,3rd ed . Cornell University Press, Ithaca, NY.

43. van Paridon, P. A., B. de Kruijff, …, K. W. Wirtz. 1986. Polyphosphoinositides undergo charge neutralization in the physiological pH range: a 31P-NMR study. *Biochim. Biophys. Acta.* 877:216–219.

44. McLaughlin, S., J. Wang, …, D. Murray. 2002. PIP(2) and proteins: interactions, organization, and information flow. *Annu. Rev. Biophys. Biomol. Struct.* 31:151–175.

45. Toner, M., G. Vaio, …, S. McLaughlin. 1988. Adsorption of cations to phosphatidylinositol 4,5-bisphosphate. *Biochemistry.* 27:7435–7443.

46. Wang, J., A. Arbuzova, …, S. McLaughlin. 2001. The effector domain of myristoylated alanine-rich C kinase substrate binds strongly to phosphatidylinositol 4,5-bisphosphate. *J. Biol. Chem.* 276:5012–5019.

47. Feller, S. E., K. Gawrisch, and A. D. MacKerell, Jr. 2002. Polyunsaturated fatty acids in lipid bilayers: intrinsic and environmental contributions to their unique physical properties. *J. Am. Chem. Soc.* 124:318–326.

48. Merz, K., B. Roux, and Biological Membranes. 1996. A Molecular Perspective from Computation and Experiment. Birkhäuser, Boston.

49. Thurmond, R. L., S. W. Dodd, and M. F. Brown. 1991. Molecular areas of phospholipids as determined by 2H NMR spectroscopy. Comparison of phosphatidylethanolamines and phosphatidylcholines. *Biophys. J.* 59:108–113.

50. Nagle, J. F. 1993. Area/lipid of bilayers from NMR. *Biophys. J.* 64:1476–1481.

51. Taylor, J., N. Whiteford, …, G. Watson. 2009. Validation of all-atom phosphatidylcholine lipid force fields in the tensionless NPT ensemble. *Biochim. Biophys. Acta.* 1788:638–649.

52. Petrache, H. I., S. W. Dodd, and M. F. Brown. 2000. Area per lipid and acyl length distributions in fluid phosphatidylcholines determined by (2)H NMR spectroscopy. *Biophys. J.* 79:3172–3192.

53. Patra, M., M. Karttunen, …, I. Vattulainen. 2003. Molecular dynamics simulations of lipid bilayers: major artifacts due to truncating electrostatic interactions. *Biophys. J.* 84:3636–3645.

54. Bradshaw, J., R. Bushby, C. Giles, and M. Saunders. 1999. Orientation of the headgroup of phosphatidylinositol in a model biomembrane as determined by neutron diffraction. *Biochemistry.* 38:8393–8401.

55. Zhou, C., V. Garigapati, and M. F. Roberts. 1997. Short-chain phosphatidylinositol conformation and its relevance to phosphatidylinositol-specific phospholipase C. *Biochemistry.* 36:15925–15931.

56. Bushby, R. J., S. J. Byard, …, D. G. Reid. 1990. The conformational behaviour of phosphatidylinositol. *Biochim. Biophys. Acta.* 1044: 231–236.

57. Hansbro, P. M., S. J. Byard, …, D. G. Reid. 1992. The conformational behaviour of phosphatidylinositol in model membranes: 2H-NMR studies. *Biochim. Biophys. Acta.* 1112:187–196.

58. Bradshaw, J. P., R. J. Bushby, …, A. Saxena. 1997. The headgroup orientation of dimyristoylphosphatidylinositol-4-phosphate in mixed lipid bilayers: a neutron diffraction study. *Biochim. Biophys. Acta.* 1329:124–138.